Supplement of Hydrol. Earth Syst. Sci., 29, 5665–5676, 2025
https://doi.org/10.5194/hess-29-5665-2025-supplement

Hydrology and Earth System Sciences
Open Access
EGU

Supplement of

Catchment landforms predict groundwater-dependent wetland sensitivity to recharge changes

Etienne Marti et al.

Correspondence to: Clément Roques (clement.roques@unine.ch)

S1: Correlation matrix between topographical parameters and seepage distribution parameters

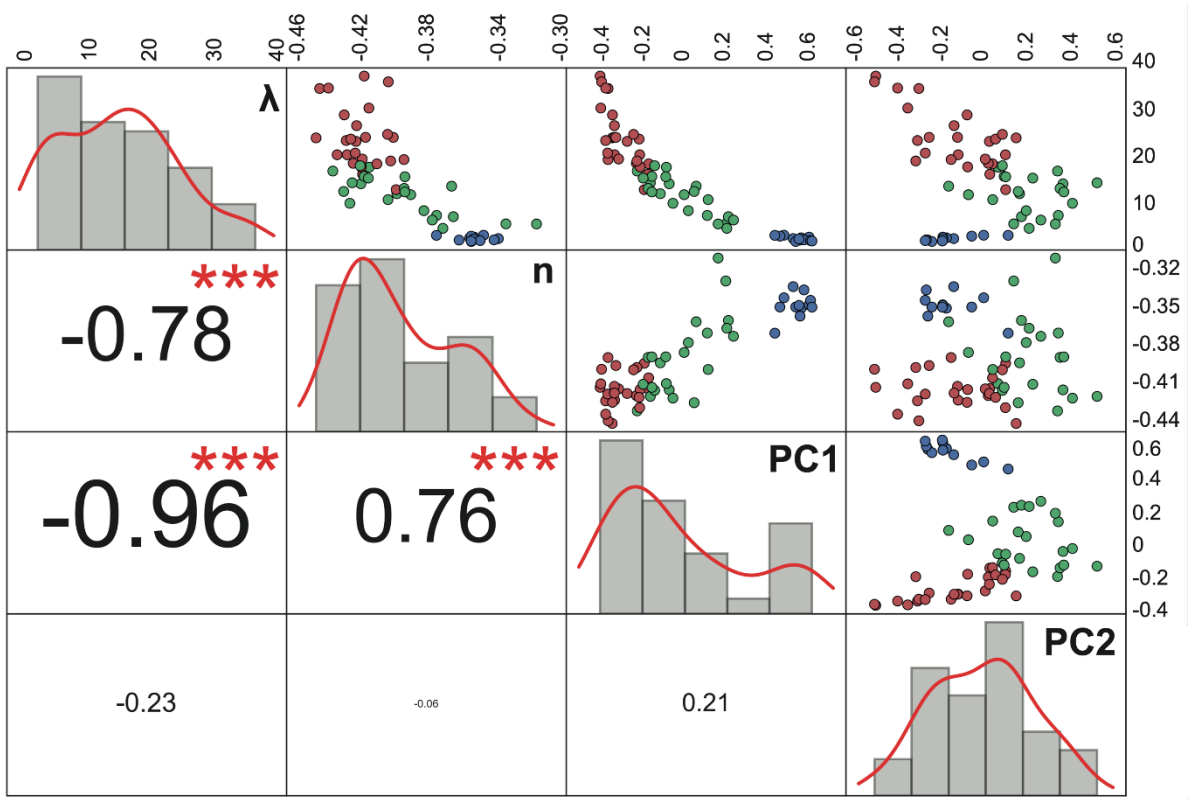

Figure S1 Correlation matrix between topographical parameters (PC1 and PC2) and seepage distribution parameters (λ and n) obtained from the curve fit. The diagonal part represents the distribution of each parameter associated with its name. The lower part indicates the correlation coefficient (r) between two variables, with stars indicating the strength of the correlation on a scale from 0 to 3 (for 3 stars p-value<0.001). The upper part represents the scatter plot between the two corresponding variables using the clusters color scheme. The X-axis is associated with both the scatter plots and the histogram distribution, while the Y-Axis is only associated with the scatter plots.

S2: Kernel Density Estimate

For the prediction of lambda, we obtained an R2 mean value of 0.835 within a 95% confidence interval defined as [0.832-0.838] and a median value of 0.858. As for n, we obtained an R2 mean value of 0.584 within a 95% confidence interval defined as [0.575-0.593] and a median value of 0.658.

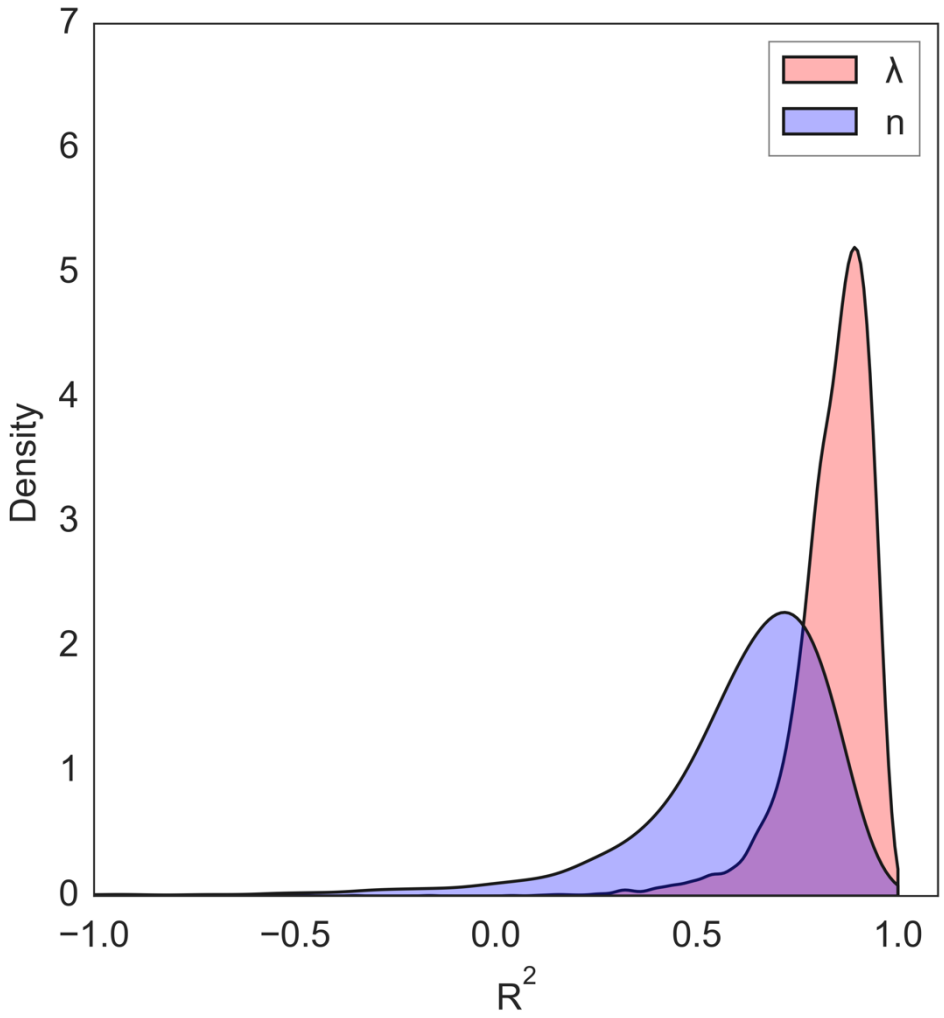

Figure S2 Kernel Density Estimate (KDE) plot depicting the coefficient of determination (R^2) for parameter estimations of λ and n using a Random Forest algorithm. Each R^2 value corresponds to one of 5000 resampling (with replacements) iterations involving 10 basins, serving as test data within a 60-basin dataset, while 50 basins were utilized for training. The sampling procedure was conducted to assess the estimation's robustness in the presence of random variations.

S3: Framework for 2D analytical solutions and sensitivity analysis of solution parameters

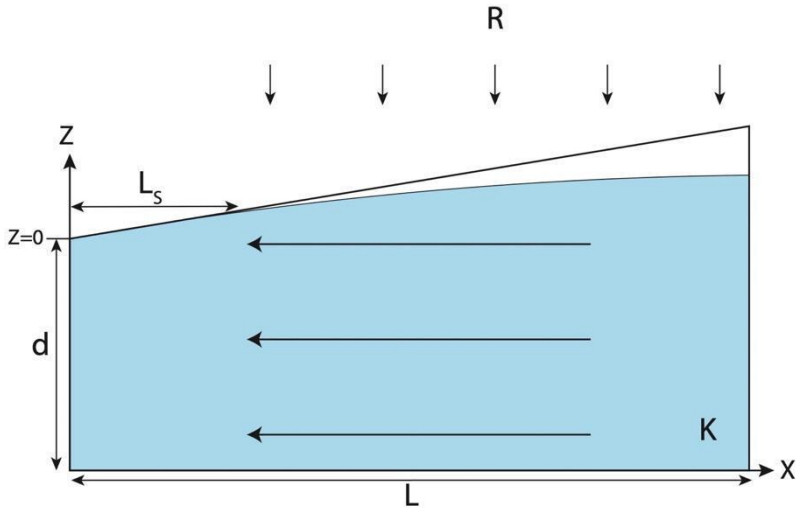

Figure S3 Illustration of the 2D hillslope model employed to define the analytical solution, based on Bresciani et al. (2014).

Bresciani et al. (2014) devised an analytical approach based on the Dupuit-Forchheimer assumption to estimate seepage length in hillslopes. This particular hillslope scenario is depicted in Figure S3, where d [L] represents the depth to the impervious base beneath the streambed, L [L] denotes the hillslope length, L_S [L] the seepage length, K [LT^{-1}] the hydraulic conductivity, R [LT^{-1}] the available recharge rate, and s [-] the topographic slope.

In this 2D hillslope framework, the model top (Z_T) is represented as a constant slope topography:

$$Z_T(x) = sx$$

with s [-] the topographic slope.

For this case the ratio between seepage length and hillslope length is defined, by mass balance, as:

$$\frac{L_S}{L} = \frac{1 - \frac{sKd}{RL}}{1 + \frac{s^2K}{R}}$$

To delve deeper into the geomorphological impact and introduce complexity beyond the constant slope framework, Bresciani et al. (2014) introduced variable slope topography, including the concave case:

$$Z_{Tconcave}(x) = sx + \frac{1}{2}bx^2$$

Or convex case:

$$Z_{Tconvex}(x) = sx - \frac{1}{2}bx^2$$

With b [-] the curvature degree.

Here, we expand this work with the Dupuit solution seepage length estimation from the three different cases. For comparison purpose, we introduce a constraint on topography borders as:

$$Z_T(x = 0) = Z_{Tconcave}(x = 0) = Z_{Tconvex}(x = 0)$$

And:

$$Z_T(x = L) = Z_{Tconcave}(x = L) = Z_{Tconvex}(x = L)$$

To take this constraint into account, we need to accommodate the expression of the concave and convex topography:

$$\Longrightarrow Z_{Tconcave}(x) = \frac{2s - bL}{2}x + \frac{1}{2}bx^2$$

$$\Longrightarrow Z_{Tconvex}(x) = \frac{2s + bL}{2}x - \frac{1}{2}bx^2$$

Resolving the same mass balance as for the linear case, for the concave and convex cases, the seepage length (L_S/L) is determined as the real roots of the following 3rd degree polynomials:

For concave case:

$$\frac{1}{2}(bL)^2\left(\frac{L_S}{L}\right)^3 + \frac{3bL(2s - bL)}{4}\left(\frac{L_S}{L}\right)^2 + \left(\frac{R}{K} + \frac{(2s - bL)^2}{4} + \frac{d}{L}bL\right)\left(\frac{L_S}{L}\right) + \frac{(2s - bL)}{2}\frac{d}{L} - \frac{R}{K} = 0$$

For convex case:

$$\frac{1}{2}(bL)^2\left(\frac{L_S}{L}\right)^3 - \frac{3bL(2s+bL)}{4}\left(\frac{L_S}{L}\right)^2 + \left(\frac{R}{K} + \frac{(2s+bL)^2}{4} - \frac{d}{L}bL\right)\left(\frac{L_S}{L}\right) + \frac{(2s+bL)}{2}\frac{d}{L} - \frac{R}{K} = 0$$

In this study, our primary focus was on the L_S/L ratio in comparison to the K/R ratio. To comprehensively investigate the analytical solution, we conducted a sensitivity analysis on the slope parameter, which serves as the most significant indicator of topography in this specific case. For this analysis, the hillslope length (L) was set to 1000m, and the depth to impervious base (d) was maintained at d=100m to respect the ratio d/L=0.1 and to consider the Dupuit Forchheimer condition (d/L < 0.2) (Bresciani et al., 2014; Haitjema & Mitchell-Bruker, 2005). We considered a range of slope values, spanning [0.02, 0.05, 0.1, 0.15, 0.2, 0.25, 0.3, 0.4].

To further explore the effects of these cases, we conducted a sensitivity study on the curvature degree. For this analysis, we maintained a fixed slope (s=0.2), and the curvature degree multiplied by the hillslope length (bL) was varied in the range [0.01, 0.05, 0.1, 0.15, 0.2] for the concave case and in the opposite range [-0.01, -0.05, -0.1, -0.15, -0.2] for the convex case.

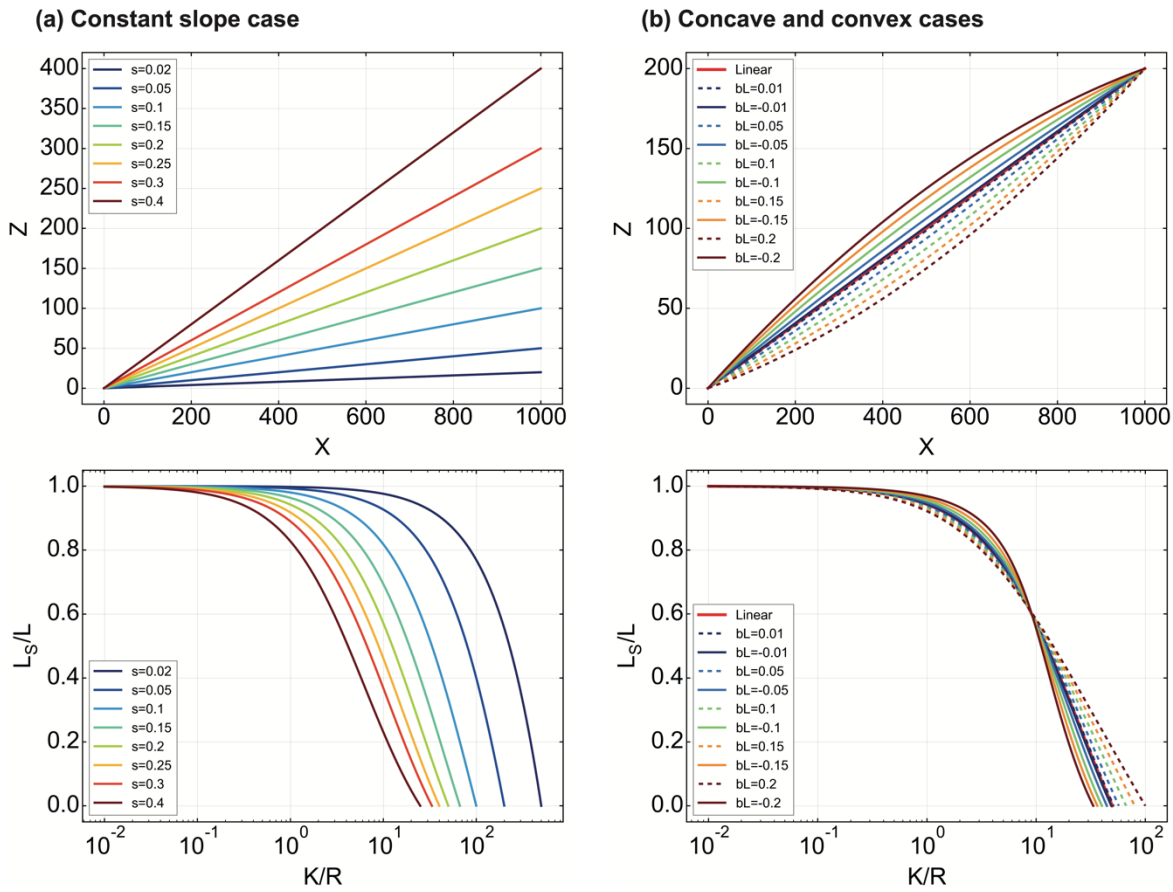

Figure S4 (a) Left upper panel: Topography of the hillslope Z_T with each color corresponding to a different slope value. Left lower panel: Seepage length ratio L_S/L plotted against the ratio R/K for each hillslope case presented on the left upper panel using the same color palette. (b) Right upper panel: Topography of the hillslope Z_T with each color corresponding to a different curvature degree value. Dashed lines represent concave cases, and solid lines represent convex cases. The linear case is represented by a solid red line. Right lower panel: Seepage length ratio L_S/L plotted against the ratio R/K for each hillslope case presented on the right upper panel, using the same color palette and line patterns.

Figure S4 presents the results of the sensitivity study with the slope (s) for the left panel and curvature degree (bL) on the right panel. The lower panel of Figure S4 presents the ratio L_S/L for the various topography described on the upper panel plotted against the ratio K/R. Regarding the varying slope (s) on the left panel of Figure S4, the results show that slope incrementation exhibits a linear effect, with gentler slopes remaining fully saturated for a higher number of K/R and reaching L_S/L =0 for the highest value of K/R. In contrast, steeper slopes desaturate at lower K/R and intercept L_S/L =0 for the smallest value of K/R. The right panel of Figure S4 displays the results for the concave and convex cases. In terms of seepage

length, we observed distinct behaviors between concave and convex topography, with more pronounced effects as the degree of curvature increased. In the convex hillslope case, remains fully saturated for a higher K/R, but the desaturation rate become quicker, leading to full desaturation ($L_S/L=0$) before the linear case. Conversely, desaturation occurred earlier in the concave hillslope cases (lower K/R), but with a slower rate, indicating that they reached total desaturation ($L_S/L=0$) beyond the linear case.

Overall, we noticed that the curvature degree has a secondary influence on the seepage length compared to the slope value (Figure S4 left versus right panel). Nevertheless, there is a noteworthy effect of the curvature degree on the desaturation rate of the hillslope.